UNIVERSITY OF BIRMINGHAM

Photonic crystal flakes

Yetisen, Ali K.; Butt, Haider; Yun, Seok-hyun

Document Version
Peer reviewed version

Link to publication on Research at Birmingham portal

Photonic Crystal Flakes

Ali K. Yetisen,[†, ‡, *] Haider Butt,[§] and Seok-Hyun Yun[†,‡,*]

[†] Harvard Medical School and Wellman Center for Photomedicine, Massachusetts General Hospital, 65 Landsdowne Street, Cambridge, Massachusetts 02139, USA

[‡] Harvard-MIT Division of Health Sciences and Technology, Massachusetts Institute of Technology, Cambridge, Massachusetts 02139, USA

[§] Nanotechnology Laboratory, School of Engineering Sciences, University of Birmingham, Birmingham B15 2TT, UK

ABSTRACT: Photonic crystals (PCs) have been traditionally produced on rigid substrates. Here, we report the development of free-standing one dimensional (1D) slanted PC flakes. A single pulse of a 5 ns Nd:YAG laser (λ=532 nm, 350 mJ) was used to organize silver nanoparticles (10-50 nm) into multilayer gratings embedded in ~10 μm poly(2-hydroxyethyl methacrylate-*co*-methacrylic acid) hydrogel films. The 1D PC flakes had narrow-band diffraction peak at ~510 nm. Ionization of the carboxylic acid groups in the hydrogel produced Donnan osmotic pressure and modulated the Bragg peak. In response to pH (4-7), the PC flakes shifted their diffraction wavelength from 500 nm to 620 nm, exhibiting 0.1 pH unit sensitivity. The color changes were visible to the eye in the entire visible spectrum. The optical characteristics of the 1D PC flakes were also analyzed by finite element method simulations. Free-standing PC flakes may have application in spray deposition of functional materials.

Tunable PCs have a wide range of applications including dynamic displays, mechanochromic devices, and multiplexed bioassays.[1-5] Embedding PCs in hydrogel matrixes allow finely tuning optical properties through dynamic modulation of lattice spacing.[6] The dynamic modulation is primarily achieved by inducing Donnan osmotic pressure created *via* the ionization of functional groups.[7] PC fabrication techniques include self-assembly of crystalline colloidal arrays,[8] layer-by-layer assembly,[9] self-assembly of di-block copolymers,[10] spin coating of polymers and nanocomposites,[11, 12] and etching porous silicon.[13] Although, PCs have been traditionally produced on silanized rigid substrates, it is desirable to have sensors free of substrates for industrial applications (*e.g.*, spray deposition).[14] To improve the angular intolerance, PCs have been confined into microspheres.[15] These spherical colloidal particles can be produced by evaporation-induced particle crystallization or polymerization of ordered particle crystallization arrays.[16, 17] While the spherical colloidal PCs can be formed by microfluidic devices, bulk generation of monodisperse beads is limited for practical applications.[15] Furthermore, their bottom up assembly of monodisperse nanoparticles has intrinsic defects in crystal formation and achieving accurate nanoparticle localization. Last of all, the use of ionic species in the monomer solution disrupts the lattice spacing, limiting their functionalization prior to polymerization. Hence, the development of a generic method to fabricate substrate-free PC sensors in ionizable hydrogels is highly desirable.

Here, we describe 1D PC flake sensors composed of functionalized hydrogel films. 1D PC flakes (d=5 mm) consist of multilayered silver nanoparticles (Ag° NPs) embedded in a poly(2-hydroxyethyl methacrylate-*co*-methacrylic acid) (p(HEMA-*co*-MAA)) hydrogel film. The lattice spacing of Ag° NP multilayers can be tuned from 200 nm to 300 nm. As the carboxylic acid groups in the hydrogel matrix ionize by external stimuli, the Donnan osmotic pressure increases, which results in water uptake into the p(HEMA-*co*-MAA) matrix. The change in the volumetric expansion hence the change of Ag° NP lattice spacing allows quantitative reporting of the concentration of external stimuli (Figure 1). The grating acts as a 1D PC and diffracts narrow-band light within the visible spectrum. In contrast to the PCs on hydrogel matrixes that expand in one dimension, free-standing hydrogels expand in two dimensions and exhibit different expansion characteristics. To explain its expansion properties, we demonstrate a 1D finite element model. The sensors can be utilized as free-standing flakes or integrated with paper or nitrocellulose membranes as strip tests for application in point-of-care diagnostics.
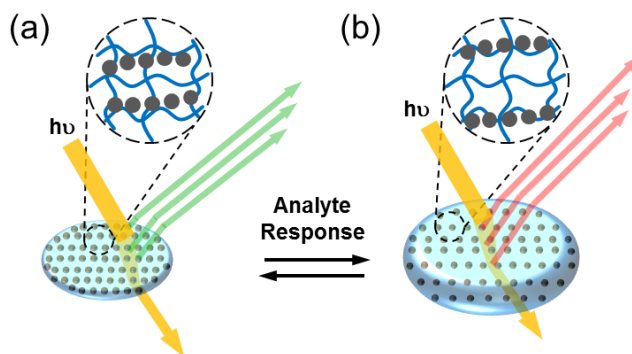
Figure 1. Operation principle of a free-standing 1D PC flake. (a) Free-standing flake in solution. (b) Expansion of the flake upon contact with external stimuli.

To create 1D PC flakes, a hydrogel matrix was prepared. A monomer solution consisting of 2-hydroxyethyl methacrylate (HEMA) (91.5 mol%), ethylene dimethacrylate (EDMA) (2.5 mol%), and methacrylic acid (MAA) (6 mol%) was prepared to from the prepolymer solution (Supporting Information 'Formulation of the monomer mixture'). These monomers were chosen as they provided flexibility for dynamically tuning the functionalized hydrogel matrix, in which carboxylic acid served as the pH-

sensitive group.[18] To form the PCs on a levelled surface and then flake off the PCs after polymerization, casted poly(methyl methacrylate) (PMMA) without birefringence was chosen as the temporary substrate. O_2 plasma treatment under vacuum rendered the surface of the PMMA hydrophilic (Figure 2a, Supporting Information 'Preparation of the substrate'). Surface modification allowed free radical UV polymerization of the monomer mixture on the PMMA surface to form a ~10 µm thick p(HEMA-*co*-MAA) film (Figure 2b, Supporting Information 'Synthesis of p(HEMA-*co*-MAA) films').
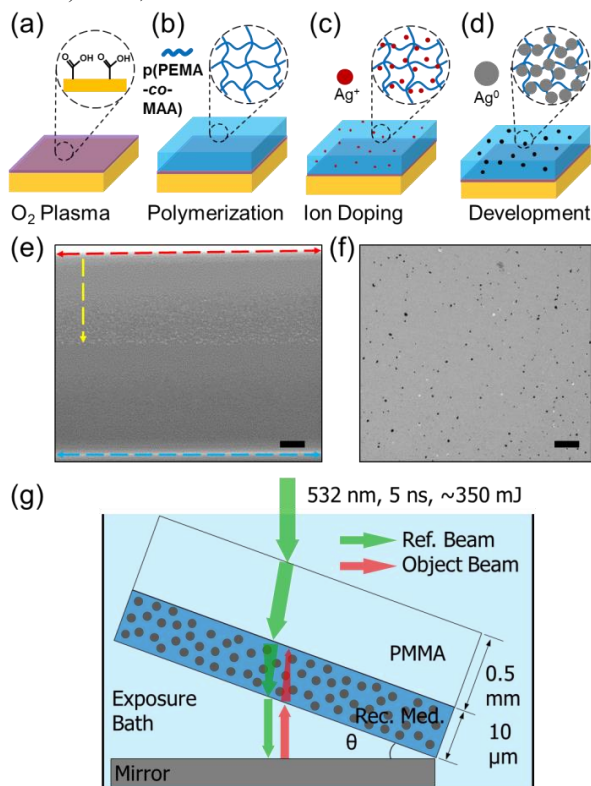

Figure 2. Laser writing of free-standing 1D PC flake sensors. (a) Treatment of the PMMA surface with O_2 plasma to render the surface hydrophilic. (b) Free radical co-polymerization of HEMA, EDMA, and MAA on the O_2-plasma-treated PMMA substrate. (c) Diffusion of Ag^+ ions into the p(HEMA-*co*-MAA) matrix. (d) The formation of Ag^0 NPs within the matrix through reduction of Ag^+ ions using a photographic developer. (e) ESEM image of the PC cross section. The red, yellow and blue dashed lines represent the surface of the matrix, the approximate depth of Ag^0 NP penetration into the matrix, and the matrix-substrate interface, respectively. Scale bar=1 µm. (f) TEM image of polymer cross-section. Scale bar=500 nm. (g) Laser writing of 1D PC within the matrix *via* a single 5 ns Nd:YAG pulse.

Ag° NPs were embedded into the p(HEMA-*co*-MAA) matrix to create a recording medium that can efficiently absorb laser light. AgNO3 salt was chosen as the Ag^+ ion source as it could be dissolved without organic solvents. AgNO3 (1.0 M) was allowed to diffuse into the p(HEMA-*co*-MAA) matrix, followed by drying (Figure 2c, Supporting Information 'Fabrication of the recording medium'). This procedure allowed immobilizing Ag^+ ions in the p(HEMA-*co*-MAA) matrix. A photographic developer (pH ~13.0) was used to reduce Ag^+ ions to metallic Ag^0 NPs within the p(HEMA-*co*-MAA) matrix (Figure 2d). The matrix was immersed in acetic acid (5% v/v, pH < 4.0,) to neutralize the developer in the matrix. Environmental Scanning Electron Microscopy

(ESEM) was used to image the cross section of the p(HEMA-*co*-MAA) matrix (Supporting Information 'ESEM Imaging'). 1D PCs were cross-sectioned using a microtome. Figure 2e shows that the Ag^0 formed in the matrix was about ~6-7 µm deep measured from the p(HEMA-*co*-MAA) surface plane to the center of the matrix cross section. Transmission Electron Microscopy (TEM) analysis indicated that the diameter of the Ag^0 NPs were 34 ± 23 nm (n=96) (Figure 2f, Supporting Information 'TEM Imaging').

1D PC flakes were fabricated using a 5 ns Nd:YAG pulsed laser (λ=532 nm, 350 mJ). A levelled Petri dish, with a front-surface silver mirror on the bottom surface, was filled with an exposure bath solution. The p(HEMA-*co*-MAA) matrix side facing down, the sample was immersed in the bath at an inclination of 5° from the surface plane of the mirror. The p(HEMA-*co*-MAA) matrix was exposed to a single 5 ns pulse (Q-switch delay: 258 µs) having a spot size of 2.5-3.5 cm (Figure 2g, Supporting Information 'Laser writing of PC flakes'). To detach the 1D PC film from the PMMA substrate, the matrix was immersed in water-ethanol solution (50%, v/v) for 1 h. After the 1D PC film floated off the PMMA substrate, the film was shaped into round PC flakes using a biopsy punch (d=5 mm). Figure 2g shows the mechanism of multilayer grating formation. The patterning of 1D PCs was achieved by creating standing waves that organized Ag^0 NPs within the p(HEMA-*co*-MAA) matrix. The matrix had an effective refractive index of ~1.37 measured by an Abbe refractometer. The interference of object and reference beams created high intensity (antinodes) and low-intensity (nodes) regions that organized the Ag^0 NPs into a multilayer.[19] The laser power, wavelength, pulse duration, NP size and surface plasmon resonance influence the efficacy of laser-writing.[20] Light-NP interaction in the standing wave can induce particle migration *via* optical forces, cause oxidation, or alter NP morphology.

To characterize the diffraction properties of the 1D photonic crystal, the grating was illuminated with the supercontinuum while light laser, and the back scattered light was recorded. Figure 3 shows the back scattered light as a function of angle of incidence, demonstrating diffraction ~510 nm. The grating diffracted light analogous to a blazed grating, in which the diffraction was an order of magnitude stronger at ~510 nm as compared to other wavelengths. Using the grating equation and measuring the position of the order from the data, the grating spacing was calculated
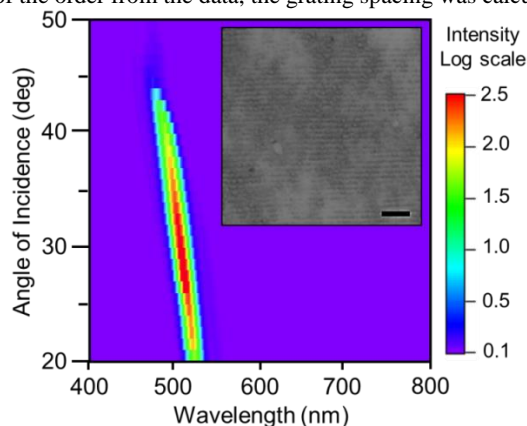

Figure 3. Optical characterization of the 1D PCs in the p(HEMA-*co*-MAA) matrix. Angle-resolved spectral measurements of the 1D PC. The inset color chart shows the intensity of the backscattered light. The inset shows a bright field image of the PC surface with transmission gratings with a periodicity of ~3 µm. Scale bar=10 µm.

as 3.01 μm. A ~10 μm thick hydrogel needs to swell a minimum of ~10 nm to cause a resolvable spectral shift. Optical images of the surface topography of 1D PCs were taken using a microscope in bright field mode. The inset in Figure 3 illustrates the transmission grating formed in the p(HEMA-*co*-MAA) matrix. The transmission grating is formed when the reference beam interferes with the beam that is reflected from the p(HEMA-*co*-MAA) matrix and water interface.[21]

The incorporation of carboxylic acid group in the matrix allowed tuning 1D PCs as the pH of the external stimuli was varied. When the pH was increased from 4 to 7 in phosphate buffers (150 mmol L^{-1}) at 24 °C, the Bragg peak of the PC flakes (6 mol% MAA) shifted from 510 nm to 620 nm. The deprotonation (ionization) of carboxylic acid functional groups increases the Donnan osmotic pressure of the hydrogel matrix.[22] As the ionization of the carboxylic acid groups was correlated with the volumetric expansion, the 1D PCs was used to quantify the pH of the external stimuli. The volumetric change induced by variation in pH was reversible. Figure 4a shows the Bragg peak shifts for PC pH sensor flakes (i) as free-standing form, (ii) on iron oxide paper composites, and (iii) on nitrocellulose membranes. The data points were fit with a modified Henderson-Hasselbalch equation to determine the apparent pK_a values of the hydrogel matrixes[23]:

$$\lambda_{\text{shift}} = \frac{\Delta\lambda}{(10^{(\text{p}K_a - \text{pH})} + 1)} \qquad \text{(Eq. 1)}$$

where λ_{shift} is the Bragg peak shift, $\Delta\lambda$ is the difference between the maximum and minimum Bragg peak wavelengths, and pK_a is the acid dissociation constant. As compared to the sensors on PMMA substrates (240 nm red shift), free-standing flakes produced a 120 nm Bragg peak shift. This shift corresponds to a pH sensitivity of 0.1 pH units based on the Henderson-Hasselbalch curve (~5 nm). However, Figure 4b shows a typical Bragg shift of a 1D PC flake as the pH was varied. Figure 4c summarizes the apparent pK_a values measured from the PC pH sensors created by different methods showing an average pK_a of 5.9 (Supporting Information Table S1).

Free-standing PC sensor flakes produced visual color changes due to variation in pH from 5.0 to 8.0 (Figure 4d, Supporting Information Figure S3). Figure 4e illustrates PC sensors integrated with iron oxide paper composites strip for monitoring pH in the metabolic range (Supporting Information 'PC assembly on iron oxide doped composite strips and nitrocellulose membranes', Figure S4-6). The Bragg peak shift by free-standing flakes was about the half of Bragg shift obtained by the pH sensors attached to the PMMA substrate. The difference in the Bragg peak shifts might be attributed to degree of freedoms that the matrix could expand. Furthermore, the pHEMA matrix can be functionalized with ionizable co-monomers to tune the pH sensing range. These co-monomers include trifluoromethylpropenoic acid (pK_a 3.00, pH range: 2-6), dimethylaminoethyl methacrylate (pK_a 8.40, pH range: 5-8), and vinyl imidazole (pK_a 5.74, pH range: 4-8). Recent advances in fluorescent sensors utilized hydrogels,[24] synthetic DNA,[25] genetically-engineered proteins,[26] antibody conjugated pH dyes,[27] and fluorescein/cyanine hybrid materials having sensitivities from 0.1 to 0.01 pH units.[28] In comparison to the demonstrated pH sensors, 1D photonic crystal flakes are label free and are immune to photobleaching. Additionally, the presented fabrication approach allows creating pH sensors at mass scale.

Finite element method was used to simulate the reflected light from the 1D PC. Figure 5a, b shows 1D photonic crystals that expand in x and y directions, respectively. The simulated transmission spectra showed that as the lattice spacing is increased from 190 to 200 nm, the diffraction spectra shifted from 510 nm

to 620 nm (Figure 5c). As the hydrogel matrix expanded in y direction (parallel to the NP layers) by 200%, Bragg peak did not shift; however, the reflection peak decreased 45 % (Figure 5d). This shows that a radial expansion of the flakes do not contribute to a change in color, it only decreases the concentration of nanoparticles per layer and decreases the diffraction efficiency.
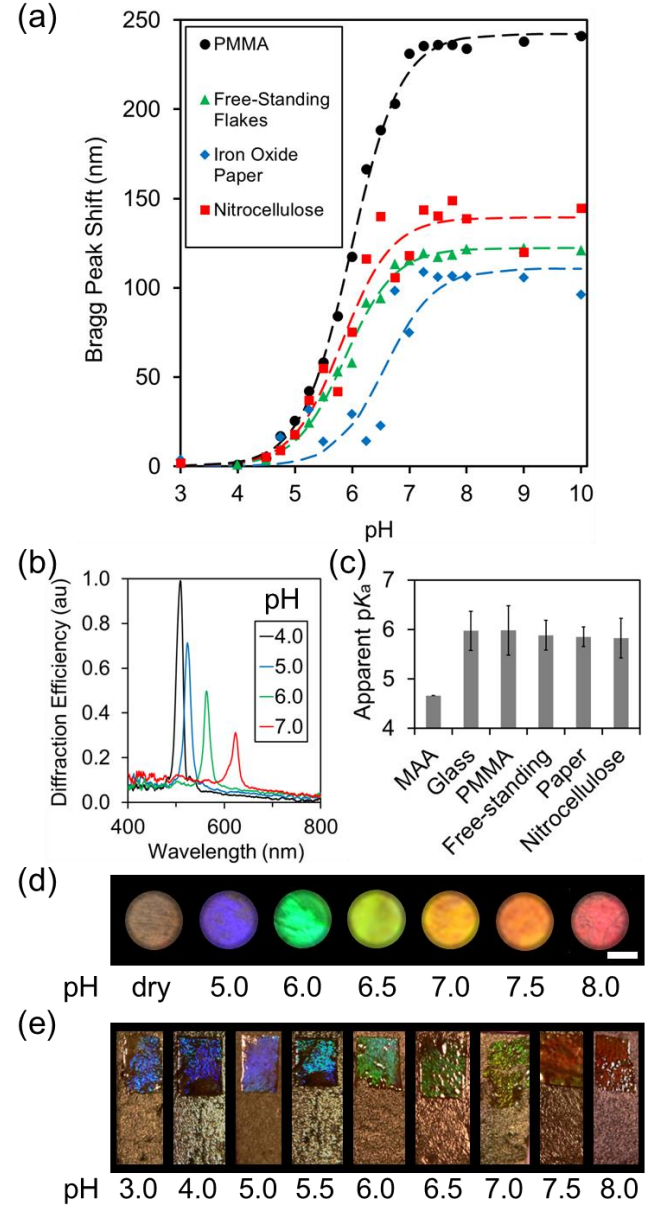

Figure 4. Spectral readouts of free-standing pH-sensitive 1D slanted PC flake sensors in phosphate buffers (150 mmol L^{-1}) at 24 °C. (a) Readouts for Bragg peak shifts as a function of pH change for flakes in free-standing, paper- and nitrocellulose-backed forms, on PMMA substrates. (b) Bragg peak shifts of the 1D PC flakes as the pH was varied from 4.0 to 7.0. (c) Apparent pK_a values of PCs in different forms. (d) Photographs of free-standing flakes from pH 5.0 to 8.0. The images were taken under white light illumination. Scale bar=3 mm. (e) Photographs of 1D PC flakes assembled on paper strips from pH 3.0 to 8.0.
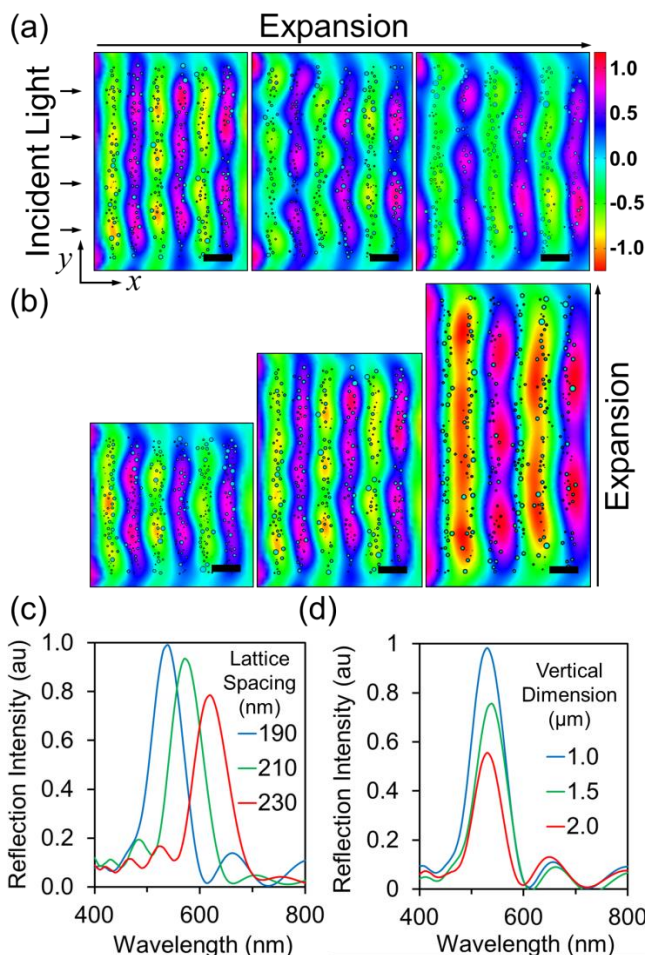
Figure 5. Finite element method simulations of 1D PC flakes. Volumetric expansion of the PC in (a) x direction (b) y direction. Scale bar = 200 nm. (c) Simulated diffraction spectrum of gratings with different lattice constants. (d) Simulated readouts of the flakes with increasing vertical dimensions (1 to 2 μm) having the same number of NPs per stack.

CONCLUSIONS

The fabrication of 1D PCs as free-standing flake sensors with a single pulse of a 5 ns laser light at 532 nm was demonstrated. The 1D PC flakes comprising of multilayer Ag^0 NPs in the p(HEMA-*co*-MAA) produced narrow-band Bragg diffraction in the entire visible spectrum. The Bragg peak of the 1D PC flakes shifted ~120 nm as the pH was increased from 4 to 8. This swelling effect was half of Bragg peak shift seen in pH sensors attached to a PMMA substrate. The difference in the dynamic Bragg peak shift might be attributed to degree of freedoms to expand. Then integration of 1D PC flakes with iron oxide/paper composites and nitrocellulose-based strip was also demonstrated. The tested paper strips showed color changes in the entire visible spectrum. The demonstrated free-standing 1D PC flakes have potential applications in spray deposition of functional materials.

ASSOCIATED CONTENT

Supporting Information

The Supporting Information is available free of charge on the ACS Publications website.

Formulation of the monomer mixture, substrate preparation, synthesis of p(HEMA-*co*-MAA) films, fabrication of the re-

cording medium, ESEM and TEM imaging, laser writing of PCs, PC assembly on iron oxide doped composite strips and nitrocellulose membranes (PDF).

AUTHOR INFORMATION

Corresponding Author

* ayetisen@mgh.harvard.edu, syun@mgh.harvard.edu

ACKNOWLEDGMENT

REFERENCES

1. Lee, H.; Kim, J.; Kim, H.; Kim, J.; Kwon, S. Colour-barcoded magnetic microparticles for multiplexed bioassays. *Nat. Mater.* 2010, 9, 745-749.
2. Han, M. G.; Shin, C. G.; Jeon, S.-J.; Shim, H.; Heo, C.-J.; Jin, H.; Kim, J. W.; Lee, S. Full Color Tunable Photonic Crystal from Crystalline Colloidal Arrays with an Engineered Photonic Stop-Band. *Adv. Mater.* 2012, 24, 6438-6444.
3. Ye, B.; Ding, H.; Cheng, Y.; Gu, H.; Zhao, Y.; Xie, Z.; Gu, Z. Photonic Crystal Microcapsules for Label-free Multiplex Detection. *Adv. Mater.* 2014, 26, 3270-3274.
4. Cai, Z.; Smith, N. L.; Zhang, J.-T.; Asher, S. A. Two-dimensional photonic crystal chemical and biomolecular sensors. *Anal. Chem.* 2015, 87, 5013-5025.
5. Howell, I. R.; Li, C.; Colella, N. S.; Ito, K.; Watkins, J. J. Strain-tunable one dimensional photonic crystals based on zirconium dioxide/slide-ring elastomer nanocomposites for mechanochromic sensing. *ACS Appl. Mater. Interfaces* 2015, 7, 3641-3646.
6. Fenzl, C.; Hirsch, T.; Wolfbeis, O. S. Photonic Crystals for Chemical Sensing and Biosensing. *Angew. Chem. Int. Ed.* 2014, 53, 3318-3335.
7. Ge, J.; Yin, Y. Responsive photonic crystals. *Angew. Chem. Int. Ed.* 2011, 50, 1492-1522.
8. Kim, S.-H.; Lee, S. Y.; Yang, S.-M.; Yi, G.-R. Self-assembled colloidal structures for photonics. *NPG Asia Mater.* 2011, 3, 25-33.
9. Wang, Y.; Angelatos, A. S.; Caruso, F. Template Synthesis of Nanostructured Materials via Layer-by-Layer Assembly. *Chem. Mater.* 2008, 20, 848-858.
10. Lim, H. S.; Lee, J.-H.; Walish, J. J.; Thomas, E. L. Dynamic Swelling of Tunable Full-Color Block Copolymer Photonic Gels via Counterion Exchange. *ACS Nano* 2012, 6, 8933-8939.
11. von Freymann, G.; Kitaev, V.; Lotsch, B. V.; Ozin, G. A. Bottom-up assembly of photonic crystals. *Chem. Soc. Rev.* 2013, 42, 2528-2554.
12. Liu, J.; Redel, E.; Walheim, S.; Wang, Z.; Oberst, V.; Liu, J.; Heissler, S.; Welle, A.; Moosmann, M.; Scherer, T. Monolithic High Performance Surface Anchored Metal− Organic Framework Bragg Reflector for Optical Sensing. *Chem. Mater.* 2015, 27, 1991-1996.
13. Bonanno, L. M.; DeLouise, L. A. Integration of a Chemical-Responsive Hydrogel into a Porous Silicon Photonic Sensor for Visual Colorimetric Readout. *Adv. Funct. Mater.* 2010, 20, 573-578.
14. Egen, M.; Braun, L.; Zentel, R.; Tännert, K.; Frese, P.; Reis, O.; Wulf, M. Artificial Opals as Effect Pigments in Clear-Coatings. *Macromol. Mater. Eng.* 2004, 289, 158-163.
15. Zhao, Y.; Shang, L.; Cheng, Y.; Gu, Z. Spherical colloidal photonic crystals. *Acc. Chem. Res.* 2014, 47, 3632-3642.
16. Zhao, X.; Cao, Y.; Ito, F.; Chen, H. H.; Nagai, K.; Zhao, Y. H.; Gu, Z. Z. Colloidal crystal beads as supports for biomolecular screening. *Angew. Chem. Int. Ed.* 2006, 45, 6835-6838.
17. Rastogi, V.; Melle, S.; Calderon, O. G.; García, A. A.; Marquez, M.; Velev, O. D. Synthesis of Light-Diffracting Assemblies from Microspheres and Nanoparticles in Droplets on a Superhydrophobic Surface. *Adv. Mater.* 2008, 20, 4263-4268.
18. Tsangarides, C. P.; Yetisen, A. K.; da Cruz Vasconcellos, F.; Montelongo, Y.; Qasim, M. M.; Wilkinson, T. D.; Lowe, C. R.; Butt, H. Computational modelling and characterisation of nanoparticle-based tuneable photonic crystal sensors. *RSC Adv.* 2014, 4, 10454-10461.
19. Yetisen, A. K.; Montelongo, Y.; Farandos, N. M.; Naydenova, I.; Lowe, C. R.; Yun, S. H. Mechanism of multiple grating formation in high-

energy recording of holographic sensors. *Appl. Phys. Lett.* 2014, 105, 261106.

20. Yetisen, A. K. Holographic pH Sensors. In *Holographic Sensors*, Springer International Publishing: Cham, Switzerland, 2015; pp 53-83.

21. Vasconcellos, F. d. C.; Yetisen, A. K.; Montelongo, Y.; Butt, H.; Grigore, A.; Davidson, C. A. B.; Blyth, J.; Monteiro, M. J.; Wilkinson, T. D.; Lowe, C. R. Printable Surface Holograms via Laser Ablation. *ACS Photonics* 2014, 1, 489-495.

22. Yetisen, A. K.; Butt, H.; da Cruz Vasconcellos, F.; Montelongo, Y.; Davidson, C. A. B.; Blyth, J.; Chan, L.; Carmody, J. B.; Vignolini, S.; Steiner, U.; Baumberg, J. J.; Wilkinson, T. D.; Lowe, C. R. Light-Directed Writing of Chemically Tunable Narrow-Band Holographic Sensors. *Adv. Opt. Mater.* 2014, 2, 250-254.

23. Po, H. N.; Senozan, N. M. The Henderson-Hasselbalch Equation: Its History and Limitations. *J. Chem. Educ.* 2001, 78, 1499.

24. Ma, J.; Ding, C.; Zhou, J.; Tian, Y. 2D ratiometric fluorescent pH sensor for tracking of cells proliferation and metabolism. *Biosens. Bioelectron.* 2015, 70, 202-208.

25. Modi, S.; Swetha, M. G.; Goswami, D.; Gupta, G. D.; Mayor, S.; Krishnan, Y. A DNA nanomachine that maps spatial and temporal pH changes inside living cells. *Nat. Nano* 2009, 4, 325-330.

26. Tantama, M.; Hung, Y. P.; Yellen, G. Imaging Intracellular pH in Live Cells with a Genetically Encoded Red Fluorescent Protein Sensor. *J. Am. Chem. Soc.* 2011, 133, 10034-10037.

27. Grover, A.; Schmidt, B. F.; Salter, R. D.; Watkins, S. C.; Waggoner, A. S.; Bruchez, M. P. Genetically Encoded pH Sensor for Tracking Surface Proteins through Endocytosis. *Angew. Chem. Int. Ed.* 2012, 51, 4838-4842.

28. Chen, Y.; Zhu, C.; Cen, J.; Bai, Y.; He, W.; Guo, Z. Ratiometric detection of pH fluctuation in mitochondria with a new fluorescein/cyanine hybrid sensor. *Chem. Sci.* 2015, 6, 3187-3194.

Table of Contents Graphic